

Polymer nanocomposites for electrocaloric refrigeration: Applications and research advances

Hongtian Li(黎洪天), Feifan Yang(杨非凡), Shenglin Jiang(姜胜林), Kanghua Li(李康华), and Guangzu Zhang(张光祖)

Citation: Chin. Phys. B, 2026, 35 (**7**): 070702. DOI: 10.1088/1674-1056/ae48ba
http://cpb.iphy.ac.cn; http://iopscience.iop.org/cpb

What follows is a list of articles you may be interested in

Electrocaloric thermal management devices: Toward high-efficiency solid-state refrigeration

Yiwen Bo(薄轶文) and Rujun Ma(马儒军)
Chin. Phys. B, 2026, 35 (**7**): 070701. DOI: 10.1088/1674-1056/ae3309

Loading uniform Ag_3PO_4 nanoparticles on three-dimensional peony-like WO_3 for good stability and excellent selectivity towards NH_3 at room temperature

Xingyan Shao(邵星炎), Fuchao Jia(贾福超), Tingting Liu(刘婷婷), Jiancheng Liu(刘健诚), Xiaomei Wang(王小梅), Guangchao Yin(尹广超), Na Lv(吕娜), Tong Zhou(周通), Ramachandran Rajan, and Bo Liu(刘波)
Chin. Phys. B, 2023, 32 (**8**): 080703. DOI: 10.1088/1674-1056/ac98a0

Thermal desorption characteristic of helium ion irradiated nickel-base alloy

Shasha Lv(吕沙沙), Rui Zhu(朱睿), Yumeng Zhao(赵雨梦), Mingyang Li(李明阳), Guojing Wang(王国景), Menglin Qiu(仇猛淋), Bin Liao(廖斌), Qingsong Hua(华青松), Jianping Cheng(程建平), Zhengcao Li(李正操)
Chin. Phys. B, 2020, 29 (**4**): 040704. DOI: 10.1088/1674-1056/ab7e99

Thermal characterization of GaN heteroepitaxies using ultraviolet transient thermoreflectance

Kang Liu(刘康), Jiwen Zhao(赵继文), Huarui Sun(孙华锐), Huaixin Guo(郭怀新), Bing Dai(代兵), Jiaqi Zhu(朱嘉琦)
Chin. Phys. B, 2019, 28 (**6**): 060701. DOI: 10.1088/1674-1056/28/6/060701

TOPICAL REVIEW — Multiferroicity and multicaloric effects

Polymer nanocomposites for electrocaloric refrigeration: Applications and research advances

Hongtian Li(黎洪天), Feifan Yang(杨非凡), Shenglin Jiang(姜胜林), Kanghua Li(李康华), and Guangzu Zhang(张光祖)†

School of Integrated Circuits, and Engineering Research Center for Functional Ceramics MOE, Huazhong University of Science and Technology, Wuhan 430074, *China*

(Received 28 November 2025; revised manuscript received 20 January 2026; accepted manuscript online 23 February 2026)

With the global surge in refrigeration demand, developing efficient, environmentally friendly solid-state refrigeration technologies is urgent. Polymer materials leveraging the electrocaloric effect (ECE) are promising alternatives to traditional vapor compression refrigeration, due to their zero global warming potential and flexibility. This review summarizes progress in polymer-based electrocaloric (EC) material composites from material design to device integration, emphasizing multiscale synergistic design as the core strategy to address polymers' inherent low thermal conductivity and high operating electric fields. We discuss ECE regulation mechanisms and synergistic effects across scales: molecular (defect engineering, high-entropy design), mesoscale (interface engineering), and macroscale (film thickness, external field control). Key challenges (low thermal conductivity, high operating fields) are analyzed, and future work should focus on precise interface engineering and multiscale structural design to advance polymer electrocaloric coolers from lab to commercialization.

Keywords: electrocaloric effect, interface engineering, high-entropy polymers, nanocomposites

PACS: 07.20.–n, 85.50.–n, 77.84.–s, 77.90.+k

DOI: 10.1088/1674-1056/ae48ba **CSTR:** 32038.14.CPB.ae48ba

1. Introduction

Recently, global temperatures have been continuously rising, with frequent occurrences of extreme weather events. The contradiction between global climate change and the surging cooling demand has become increasingly intensified. Traditional vapor compression refrigeration relies on hydrofluorocarbon (HFC) refrigerants, whose emissions exhibit high global warming potential. Meanwhile, electricity consumption associated with cooling indirectly leads to substantial greenhouse gas emissions. It is estimated that cooling demand currently accounts for approximately 10% of global electricity consumption and is projected to exceed 45% by 2050. Therefore, the development of efficient and environmentally friendly alternative refrigeration technologies is imperative.[1–3]

Various non-vapor compression refrigeration technologies have been developed, including thermoelectrics (TE),[4] magnetocaloric effect (MCE),[5] electrocaloric effect (ECE),[6,7] barocaloric effect (BCE),[8] sorption cooling,[9] and enhanced radiative cooling.[10] Among these, TE cooling has been commercialized. However, its coefficient of performance (COP) remains substantially lower than that of vapor compression systems, which limits its practical large-scale application. BCE and MCE are driven by hydrostatic pressure and magnetic fields as external stimuli, respectively to drive reversible changes in the internal entropy of materials, thereby achieving efficient heat absorption and release. Nevertheless, their operation often requires complex secondary energy conversion devices, which has hindered the miniaturization of the entire refrigeration system. In contrast, the electrically driven ECE exhibits excellent cooling performance.[11,12] Therefore, among numerous alternative technologies, the ECE is recognized as one of the most promising solid-state refrigeration technologies for replacing traditional vapor compression systems, owing to its high COP, fast response, and potential for miniaturized integration.[13]

The investigation into the ECE dates back to 1930, when this phenomenon was first observed in Rochelle salt ($NaKC_4H_4O_6{\cdot}H_2O$) by Kobeko *et al.*[14] However, the adiabatic temperature change (ΔT) achieved in these early studies was extremely low. In subsequent decades of research, materials still exhibited minimal ΔT values, failing to meet the requirements for commercial applications. It wasn't until 2006[6] and 2008[7] that the giant ECE was successively discovered in the inorganic material $PbZr_{0.95}Ti_{0.05}O_3$ and the organic polymer polyvinylidene fluoride (P(VDF-TrFE)). Following this breakthrough, ECE cooling technology rapidly regained widespread attention from both academia and industry. Subsequently, research on ferroelectric refrigeration materials flourished, with studies mainly focusing on three categories: inorganic materials, organic materials, and inorganic–organic composites. Representative examples include per-

†Corresponding author. E-mail: zhanggz@hust.edu.cn

© 2026 Chinese Physical Society and IOP Publishing Ltd. All rights, including for text and data mining, AI training, and similar technologies, are reserved.

ovskite ferroelectric ceramics, PVDF-based polymers, and their composites.[15–17] In particular, PVDF-based polymers have emerged as a research hotspot owing to their flexibility, processability, and high breakdown field strength properties that make them particularly suitable for applications including wearable devices and chip thermal management.[18,19]

However, significant challenges remain in the practical implementation of polymer ECE systems. The first and most critical challenge is the inherent limitation of polymers' electrical properties: high electric fields close to the breakdown limit are often required to achieve ΔT, which compromises device reliability.[20–22] Additionally, the relatively low thermal conductivity of polymer materials ($\sim$ 0.1–0.5 $\mathrm{W{\cdot}m^{-1}{\cdot}K^{-1}}$) severely limits the heat transfer of devices. To address these bottlenecks, the focus of research has shifted to polymer composite materials. By incorporating inorganic functional fillers, synergistic improvements in both electrical and thermal management performance can be achieved.[19,23,24]

This review is intended to systematically summarize the latest advancements in polymer nanocomposites for electrocaloric refrigeration from a multi-scale perspective. It focuses on clarifying the performance regulation mechanisms spanning from the molecular scale to the device scale, assesses the design principles and performance limitations of innovative electrocaloric devices, and highlights future research directions.

2. Principles and measurement of the electrocaloric effect

The core principle of the ECE is that dielectric materials become polarized under a time-varying external electric field, and the resulting isothermal entropy change (ΔS) induces reversible temperature fluctuations. Similar to traditional vapor compression refrigeration (VCR) technology, ECE refrigeration is also based on the "cyclic heat pumping" mechanism (Fig. 1(a)) and follows thermodynamic cycles including the Brayton and Ericsson cycles (Fig. 1(b)). The key distinction is that the ECE utilizes the dipole ΔS of solid dielectric materials instead of the liquid–vapor phase transition that occurs in VCR systems.[11,25]

As shown in Fig. 1(a), the simplest cyclic behavior of ECE can be described using the Brayton cycle. During stages 1–2, the system is in an initial state with no electric field applied ($E = 0$), where electric dipoles in the EC material are randomly oriented at ambient temperature T_0. Under adiabatic conditions, an electric field is applied, inducing the alignment of dipoles along the field direction and a concomitant reduction in dipole entropy. Owing to the conservation of total system entropy, the material temperature rises rapidly to T_h. During stages 2–3, the electric field is maintained at $E = E_0$, with the temperature of the EC material sustained above the ambient temperature. Heat is dissipated to the environment via heat exchange, thereby gradually restoring the material temperature to T_0, while the low dipole entropy level is retained. During stages 3–4, the electric field is switched off ($E = 0$) under adiabatic conditions. The dipoles transition from an ordered state to a disordered state, resulting in an increase in dipole entropy and an abrupt decrease in material temperature to T_c. During stage 4–1, with $E = 0$ kept constant, the cooled EC material absorbs heat from the heat source, raising its temperature back to T_0 with a simultaneous increase in dipole entropy. The system then returns to its initial state. By repeating this cycle, heat can be continuously transferred from the heat source to the heat sink.[25]

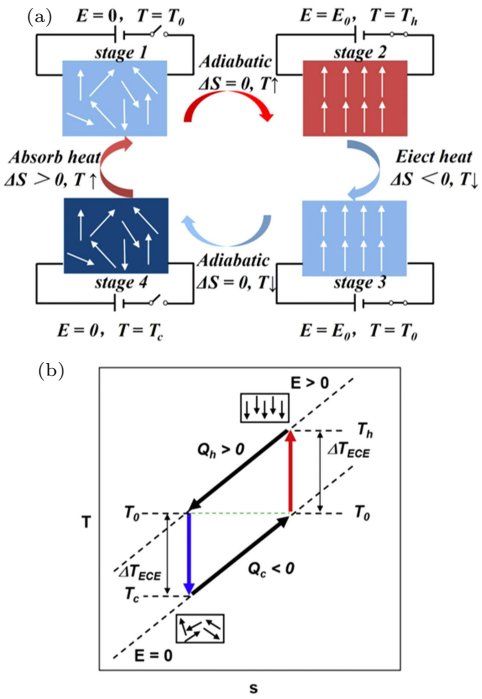


Fig. 1. Process of an electrocaloric cooling cycle. (a) A caloric-cooling cycle in an EC element. Arrows in the box indicate dipole orientation. Temperatures of both heat sink and heat source are assumed to be the same as T. The numbers 1, 2, 3, and 4 indicate different stages in a cycle.[16,19,26] (b) Thermodynamic cycle.[26] Copyright 2023, Elsevier.

At present, the testing methods for the ECE are primarily categorized into indirect and direct measurement approaches. The ECE in ferroelectric materials is usually interpreted using the Landau–Devonshire (L–D) theory.[27,28] This yields expressions for the ΔT and ΔS. For a ferroelectric material, these can be formulated as[27]

$$\Delta S = -\frac{1}{2}\beta\left[P^2(E_2) - P^2(E_1)\right] = -\frac{1}{2}\beta P^2, \tag{1}$$

$$\Delta T = \frac{1}{2C_E}\beta T P^2, \tag{2}$$

where E_1 and E_2 are defined as the initial and final electric fields, respectively, and C_E is referred to as the heat capacity at constant electric field. Polarization (P) and Landau coefficient

(β) can be obtained via ferroelectric characterization tests and measurements of the dielectric's Curie constant. However, the uniform polarization field assumed in the standard L–D theory is perturbed by heterogeneous interfaces and nanoscale fillers, which often induces relaxor-like behavior and complex local field distributions not accounted for by the model's predefined parameters.[29,30] In practice, the indirect method based on Maxwell relations is more widely adopted for thin films, and the derivation of this method is provided as follows:[27,31]

$$\Delta T = -\frac{1}{\rho}\int_{E_1}^{E_2}\frac{T}{C_E}\left(\frac{\partial p}{\partial T}\right)_{E,X}\mathrm{d}E \tag{3}$$

$$\Delta S = \int_{E_1}^{E_2}\left(\frac{\partial p}{\partial T}\right)_{E,X}\mathrm{d}E, \tag{4}$$

where ρ is the material density. The accuracy of this method is dependent on two key inputs: temperature-dependent C_E, in conjunction with reliable P data from P–E loops. This approach is valid for canonical ferroelectrics but presents inherent challenges for the target polymer nanocomposites. Relaxor ferroelectrics (RFE) and composites with strong interfacial polarization exhibit dynamic, history-dependent polarization characteristics arising from ergodic or non-ergodic dynamics, a behavior that is further exacerbated by interfacial effects. As such, the P obtained from standard P–E loops fails to reflect the true equilibrium state, thereby introducing substantial errors into Eqs. (3) and (4).

Thus, the selection of indirect versus direct measurement methods for polymer nanocomposites is of critical importance. Indirect methods are applicable to materials with stable field-dependent polarization behavior, whereas direct calorimetric or thermometric measurements are indispensable for novel composites or those exhibiting strong relaxor characteristics and interfacial effects, thus ensuring the reliability of performance benchmarking.

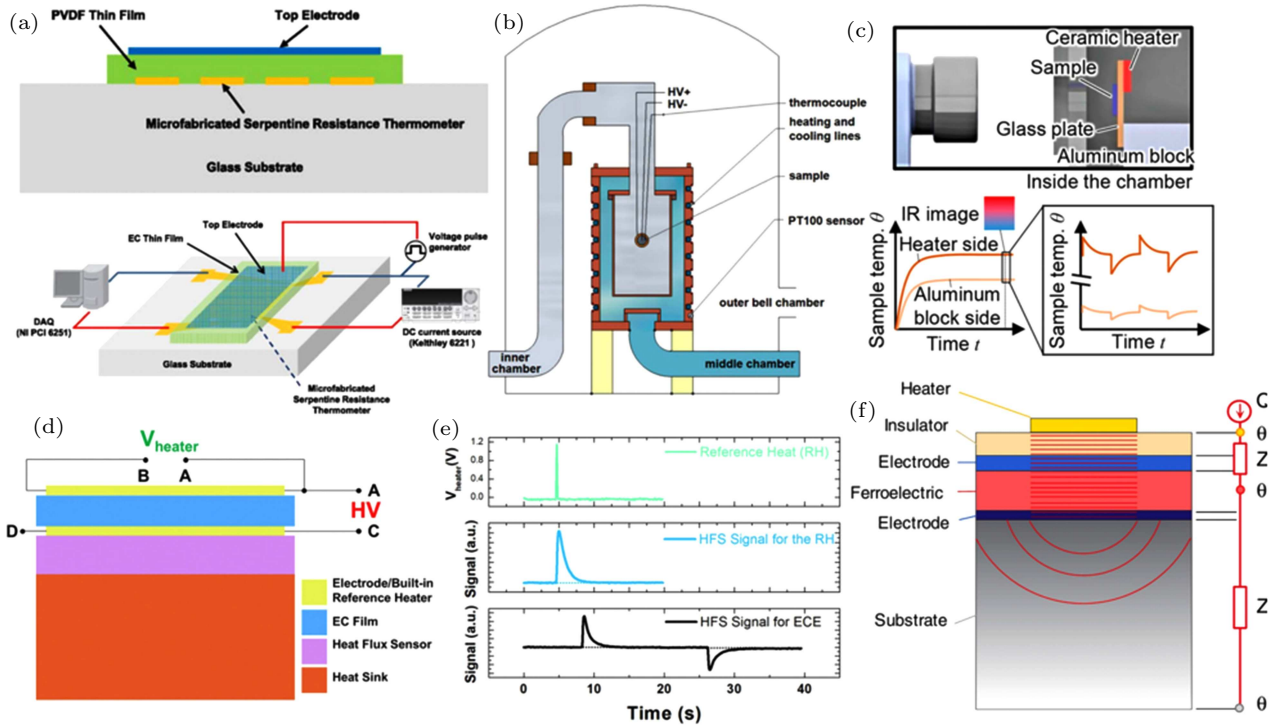


Fig. 2. Direct measurement and calibration methods for the ECE. (a) Thermistor.[32] Copyright 2013, AIP Publishing. (b) Thermocouples.[33] Copyright 2018, AIP Publishing. (c) Infrared camera.[35] Copyright 2021, AIP Publishing. (d) and (e) *In situ* calibrated ECE measurement protocol.[16] Copyright 2019, Elsevier. (f) 3-omega method.[39] Copyright 2017, American Physical Society.

Direct measurement methods directly capture changes in temperature or heat flux during electric field cycling through highly sensitive sensors, such as thermistors (Fig. 2(a)),[32] thermocouples (Fig. 2(b)),[33] infrared cameras (Fig. 2(c)),[34,35] or modified commercial differential scanning calorimeters (DSC), which yield more intuitive and reliable results. However, issues including contact between temperature sensors and samples, as well as heat exchange between test samples and the surrounding environment, remain. Consequently, the direct testing method faces two major challenges: The first challenge is the absence of standardized samples. EC materials are often integrated with non-active components such as electrodes and wires, which act as thermal loads to absorb heat. This results in the underestimation of EC material performance.[16] The second challenge is the difficulty in testing thin-film samples. The thickness of polymer ECE films is typically less than 1 μm. During direct measurement, the ΔT induced by the ECE of the polymer itself is small, while the substrate supporting the film produces a substantial thermal load, which severely impairs test accuracy. To address these issues, various calibration methods and high-sensitivity measurement techniques have been developed by

researchers.[36] Qian *et al.*[16] have developed an *in-situ* Joule heating calibration method, as shown in Fig. 2(d). By establishing a quantitative relationship for thermal signals via an integrated reference heater, their method significantly improves the consistency and comparability of measurement results across different laboratories.[37,38] To tackle the challenges in thin-film testing, micro-nano thermal characterization techniques, such as micro-thermography,[32] 3-Omega technology (Fig. 2(f)),[39] and scanning thermal microscopy (SThM),[40] have opened new avenues for the precise, *in-situ* characterization of ECE. These methods achieve temperature sensitivities down to the millikelvin (mK) level. Nevertheless, the field of electrocaloric measurement still lacks unified standards. Future work should focus on developing standardized testing protocols and error assessment systems.

3. EC composite materials under multi-scale collaborative regulation strategy

Polymer electrocaloric materials face two key challenges for practical use: the need for high electric fields near the breakdown limit to induce significant adiabatic ΔT, and inherently low thermal conductivity that restricts device heat exchange efficiency. To address this bottleneck, research has shifted from single-component exploration to multi-scale synergistic regulation (molecular, mesoscopic, macroscopic). Molecular engineering underpins polarization and entropy regulation, mesoscopic design amplifies these advantages via interface and multiphase coupling, and macroscopic optimization translates microscale gains into practical device performance, thereby enabling simultaneous optimization of ECE and thermal management.

To clarify the regulatory mechanism, the core concepts are defined as follows: high-entropy states in EC polymers are categorized into three scales: the molecular scale, governed by intrinsic chain regulation, and the mesoscopic scale, dominated by multiphase and interfacial regulation. Interface effects are explicitly identified as a phenomenon exclusive to the mesoscopic scale, while the three scales (molecular scale corresponding to chain structure; mesoscopic scale referring to multiphase and interface; macroscopic scale relating to macrostructure and external fields) exhibit fully non-overlapping boundaries.

3.1. Molecular-scale engineering: defect engineering and high-entropy strategy

At the molecular scale, the core of regulation lies in optimizing the polarization response and broadening the operating temperature range, which essentially involves the precise manipulation of polymer chain structure, ordered states, and entropy variations. Traditional normal ferroelectric polymers primarily refer to P(VDF-TrFE) copolymers with different molar ratios, among which the widely studied P(VDF-TrFE) (55/45 mol%) exhibits a giant ΔT near its phase transition temperature.[7,41–43] As shown in Figs. 3(a) and 3(b), the ECE in this system was first observed by Neese *et al.*[7] via indirect measurement methods, and subsequent systematic studies confirmed that a ΔT of 12 K could be achieved near the phase transition temperature (~ 67 °C) under an applied electric field of 120 MV/m using thermistor bead measurements.[41] However, the sharp first-order phase transition of this copolymer leads to an excessively narrow effective operating temperature range, making it unsuitable for continuous room-temperature refrigeration applications.

To address this challenge, a defect engineering strategy was proposed by researchers. By introducing defects to disrupt long-range ferroelectric ordering, the material is transformed into an RFE with a diffuse phase transition. Within this RFE, polar nanodomains can realize reversible polarization reversal over a broad temperature range.[16,20,23,44] For instance, the third monomer, chlorofluoroethylene (CFE), was chemically introduced into P(VDF-TrFE) chains to synthesize the ternary copolymer P(VDF-TrFE-CFE). As a chemical defect, the CFE monomer effectively disrupts macroscopic ferroelectric domains and forms polar nano-regions. Indirect testing results showed that excellent electrocaloric performance was maintained over a broad temperature range exceeding 40 K.[7] Beyond chemical defects, physical defects also provide an effective approach to achieve the RFE transition.[45,46] For example, P(VDF-TrFE) (68/32 mol%) was irradiated with high-energy electrons; physical defects induced by irradiation in molecular chains disrupt long-range ferroelectric order, thus converting the material into an RFE. Via a high-resolution calorimeter, a giant ΔT of 20 K was achieved near room temperature (~ 33 °C) under an applied electric field of 160 MV/m (Figs. 3(c) and 3(d)).[48] Furthermore, after high-energy electron irradiation of P(VDF-TrFE) (65/35 mol%), a ΔT of 35 K was achieved under an external electric field of 180 MV/m, further validating the enhancing effect of physical defects on the giant electrocaloric effect.[46]

Notably, inorganic nanofillers offer another avenue for molecular-scale defect engineering. For TiO_2 nanofillers incorporated into the PVDF matrix, the nanoparticles not only form an interconnected polar phase network but also induce molecular-level defects in the surrounding PVDF. This synergistic effect markedly reduces the ferroelectric–paraelectric phase transition energy barrier, enabling a large reversible ferroelectric–paraelectric phase transition under a moderate electric field (40 MV/m).[47] This work expands the implementation of molecular-scale defect engineering, establishing a pioneering paradigm for modulating phase transition kinetics via direct or filler-mediated defect induction to achieve giant ECE at moderate fields. Notably, the molecular-level struc-

tural optimization (e.g., chain defect introduction, configurational entropy enhancement) provides a prerequisite for subsequent mesoscopic interface engineering — by regulating polymer chain flexibility and polarizability, it enables stronger polarization coupling between the polymer matrix and inorganic fillers at the mesoscale.

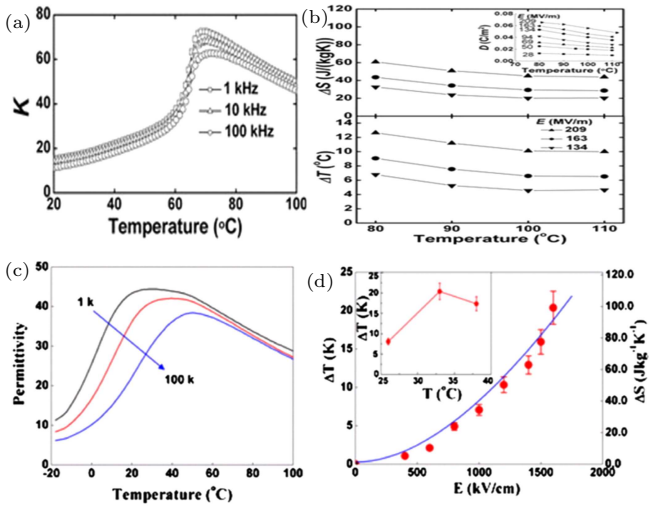


Fig. 3. The temperature-dependent permittivity spectroscopy and ECE properties: (a), (b) ferroelectrics.[7] Copyright 2008, The American Association for the Advancement of Science. (c), (d) Relaxor ferroelectrics.[48] Copyright 2010, AIP Publishing.

To further decrease the driving electric field, a high-entropy strategy derived from high-entropy alloy design was introduced into polymer electrocaloric materials. It is worth noting that the core of high-entropy alloys lies in maximizing configurational entropy through multi-component synergistic effects to optimize material properties. This concept has been innovatively extended to polymers, where entropy regulation is employed to enhance the driving force for polarization reversal, thereby enabling significant ECE under low electric fields. PVDF-based polymers form a complex system where configurational entropy, lattice entropy, and polarization entropy all contribute to ECE. Their respective contributions depend on the material's microstructure (e.g., β-phase content, crystallinity, orientation), external field conditions (e.g., electric field strength, temperature), processing techniques, and application scenarios, thus requiring specific analysis under tailored experimental contexts. Specifically, a P(VDF-TrFE-CFE-CTFE) (CTFE: chlorotrifluoroethylene) quaternary copolymer was initially developed via the enhancement of chemical component complexity, which represents a typical molecular-scale high-entropy polymer design strategy. Effective entropy-state regulation is achieved in this copolymer through the incorporation of multiple components.[49] In another study, a P(VDF-TrFE-CFE-CTFE) (DB: double bond) quaternary copolymer with low CFE content (6.6 mol%) was designed and optimized to exhibit a diffuse phase transition state adjacent to the critical point of the normal ferroelectric phase. Under an applied electric field of 100 MV/m, an isothermal ΔS of 100 J·kg^{-1}·K^{-1} was achieved. Furthermore, a large electromechanical strain of 2.75% was attained under an applied electric field of 70 MV/m. This result highlights the synergistic enhancement of ECE and electrodynamic driving performance under low electric fields via high-entropy-inspired component regulation.[50] Subsequently, another independent optimization approach focusing on chain conformational disorder was reported. As shown in Figs. 4(a) and 4(b), fluoroalkene (FA) double bonds were introduced into P(VDF-TrFE-CFE) to increase chain conformational disorder; a ΔT exceeding 7.5 K was achieved under a moderate applied electric field of 50 MV/m, as detected using an *in-situ* Joule heating calibration method.[22] This design enriches the entropy regulation toolkit for electrocaloric polymers. At the composite level, the high-entropy strategy was further extended: high-entropy alloy nanoparticles were integrated with polymers to form core-shell structures. Through this structure, the ΔS of the composite was elevated to 55 J·kg^{-1}·K^{-1}, which is 2.4 times higher than that of pure polymers (Fig. 4(c)).[51]

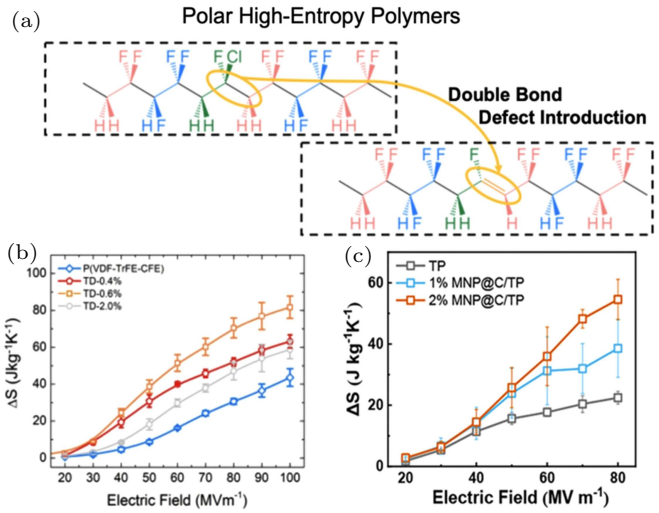


Fig. 4. (a), (b) Design and ECE properties of polar high-entropy polymers.[52] Copyright 2025, Science Exploration Press. (c) Interface polarization strategy enhances polymer conformational entropy.[21] Copyright 2023, The American Association for the Advancement of Science.

3.2. Mesoscopic-scale engineering: interface effects and multiphase structure design

Synergistic optimization of electrocaloric and thermal conductive properties is achieved at the mesoscale by constructing multiphase heterogeneous structures and controlling interface effects. Building on the polarization advantages at the molecular scale, interface engineering further amplifies ECE performance through interfacial polarization, stress modulation, and thermal conduction network construction. This scale mainly covers polymer–polymer blends and polymer–inorganic composites, whose ECE performance is summarized in Tables 1 and 2, respectively. These tables are designed to illustrate key principles for synergistic optimization. For polymer–polymer blends (Table 1), performance is de-

pendent on interphase dielectric compatibility and interfacial adhesion, with the aim of balancing enhanced interfacial polarization and retained dielectric breakdown strength. In the case of polymer–inorganic composites (Table 2), the polarization response and formation of thermal conduction pathways are strongly affected by filler dimensionality. Notably, ΔT and thermal conductivity serve as key metrics for cooling efficiency and heat dissipation, respectively. An optimal balance of these parameters is achieved in high-performance materials via tailored interface engineering.

Table 1. Summary of key properties of EC polymer-polymer blends.

Material	T (K)	ΔS (J·kg^{-1}·K^{-1})	ΔT (K)	ΔE (MV/m)	Measured	Ref.
P(VDF-TrFE)55/45 mol%	353	60.8	12.6	200	Indirect	[41]
Irradiated P(VDF-TrFE)68/32 mol%	306	95	20	160	direct	[48]
Irradiated P(VDF-TrFE)65/35 mol%	323	160	35	180	direct	[46]
P(VDF-TrFE-CFE) 59.2/33.6/7.2 mol%	303	73.5	14.8	150	direct	[53]
P(VDF-TrFE-CFE) 69.7/30.3/6 mol%	313	60	12	100	direct	[54]
P(VDF-TrFE-CFE-CTFE) 56.1/33.2/5.9/4.8 mol%	308	40	8	100	direct	[49]
Int-biased Blends (90/10) Co:65/35 mol% Ter:59/33/8 mol%	313	72	14.4	100	direct	[55]
P(VDF-TrFE-CFE)/DMHD	/	100	/	100	direct	[21]
Blends (90/10) Co: 62.5/29/8.5 mol%Ter:55/45 mol %	300	50	10	150	direct	[56]
P(VDF-TrFE-CTFE-DB)	/	100	/	100	direct	[50]
P(VDF-TrFE-CTFE)-TD	/	37.5	7.5	50	direct	[22]

Table 2. Summary of key properties of EC polymer-inorganic composites.

Material	T (K)	ΔS (J·kg^{-1}·K^{-1})	ΔT (K)	ΔE (MV/m)	Measured	Ref.
P(VDF-TrFE-CFE)/PMN-PT	303	150	31	180	direct	[57]
P(VDF-TrFE-CFE)/BNNS/BST67	303	210	50.5	250	direct	[58]
P(VDF-TrFE-CFE)/BNNSs/BST1/2/3	273–333	170	35	200	direct	[59]
P(VDF-TrFE-CFE)/AAO	room temperature	12	2.5	50	direct	[23]
P(VDF-TrFE-CFE)/BST(NWs)	room temperature	96	19.5	100	direct	[60]
P(VDF-TrFE)/BST	351	/	2.5	60	indirect	[61]
P(VDF-TrFE-CFE)/graphene	room temperature	24.8	5.2	40	direct	[62]
P(VDF-TrFE-CFE)/ BZT/nfs	303	105	44.3	200	direct	[63]
P(VDF-TrFE-CFE)/BFBZT	303	78	13.8	75	direct	[64]
P(VDF-TrFE-CFE)/ BTSn11	room temperature	44	9.08	100	indirect	[65]
P(VDF-TrFE-CFE)/BST(NF)	298	70	11.3	70	direct	[66]
P(VDF-TrFE-CFE)/SiOC	room temperature	25.4	2	30	direct	[67]

3.2.1. Electrocaloric performance of polymer-polymer blends

Synergistic enhancement in polymer blends is achieved by constructing nanoscale phase-separated structures at the interfaces of different components and utilizing differences in their dielectric properties. For instance, charge accumulation and an internal bias electric field are induced at the interface due to the difference in dielectric constant between normal ferroelectric polymers and RFE polymers. This internal bias field acts as an additional driving force for polarization, thereby enhancing the overall polarization response and room-temperature electrocaloric effect.

In early studies, a blend system composed of P(VDF-TrFE-CFE) and P(VDF-CTFE) was investigated, and a ΔT of 6 K was achieved at 318 K under an applied electric field of 120 MV/m via thermistor measurements.[68] This result confirmed the feasibility of such blends for electrocaloric applications. In subsequent studies, 10 wt% P(VDF-TrFE) (55/45 mol%) was introduced into P(VDF-TrFE-CFE) to prepare blends. Results showed that this composition not only increased the crystallinity of the blend by more than 10% but also induced a transition from normal ferroelectric behavior to RFE behavior. Via thermocouple measurements, a ΔT of 7 K was confirmed for the blend, which is a 30% enhancement compared with the pure P(VDF-TrFE-CFE) terpolymer.[56] Further investigations focused on the P(VDF-TrFE-CFE)/P(VDF-TrFE) (90/10 mol%) blend system. By utilizing the internal bias field as an additional polarization driving force, a ΔT of 4.9 K was achieved at 50 MV/m, which is a 45% enhancement compared with blends lacking such an internal bias field.[55] More notably, when the molar ratio of P(VDF-TrFE-CFE) to P(VDF-TrFE) is 50/50, interfacial coupling induces an anomalous negative electrocaloric effect. This effect allows the activation of cooling with a single electric pulse, which provides new possibilities for the development of miniature cooling cells (Figs. 5(a) and 5(b)).[69,70]

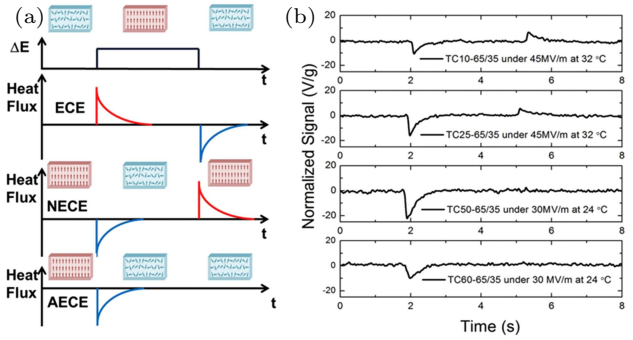


Fig. 5. (a), (b) ECE performance (ΔS and ΔT) of PVDF-TrFE 50/50 mol% in virgin/irradiated stage.[69] Copyright 2016, AIP Publishing.

3.2.2. Electrocaloric performance of polymer inorganic composites

Synergistic enhancement of both electrical performance and thermal conductivity in polymer–inorganic composites can be achieved by precisely regulating the interfacial coupling and microstructure between the polymer matrix and inorganic fillers. Mainstream inorganic fillers are high-dielectric ferroelectric ceramics, such as $Ba_{0.6}Sr_{0.4}TiO_3$ (BST) and $Pb(Mg_{1/3}Nb_{2/3})O_3$-$PbTiO_3$ (PMN-PT). These ceramics enhance the overall polarization difference (ΔP) through interfacial polarization effects, while simultaneously compensating for the low thermal conductivity of the polymer matrix.[15,18,20]

The morphological design of inorganic fillers plays a crucial role in optimizing composite performance. Numerical simulations, where $BaTiO_3$ nanoparticles were used as fillers in polymer composites, have shown that smaller filler particles increase the interfacial contact area and thus enhance polarization coupling.[71] For instance, when PMN-PT nanoparticles were used as fillers, a ΔT of 9 K was achieved under an applied electric field of 75 MV/m as measured via thermocouples. This value represents a 200% improvement compared with the pure P(VDF-TrFE-CFE) terpolymer.[57] Nanostructures with high aspect ratios (e.g., nanowires, nanofibers) are capable of forming continuous polarization pathways and thermal conduction networks even at low filler loading levels. For example, when BST nanowires were composited with P(VDF-TrFE-CFE), the resulting composite showed a 35% increase in dielectric constant and a 25% enhancement in breakdown field strength; an improvement attributed to the high aspect ratio of the nanowires. A ΔT of 19.5 K at 100 MV/m was measured via an infrared camera (Figs. 6(a) and 6(b)).[60] More notably, a composite of $Ba(Zr_{0.21}Ti_{0.79})O_3$ (BZT) nanofibers and polymer, when characterized using a high-sensitivity heat flux sensor, achieved a record ΔT of 44.3 K under an applied electric field of 200 MV/m. To clarify the interfacial mechanism, phase-field simulations were conducted to quantify the enhanced polarization region at the interface. *In-situ* piezoresponse force microscopy (PFM) observations of domain evolution confirmed that the interfacial coupling between BZT nanofibers and the polymer matrix is the primary factor driving polarization enhancement (Figs. 6(c) and 6(d)).[63]

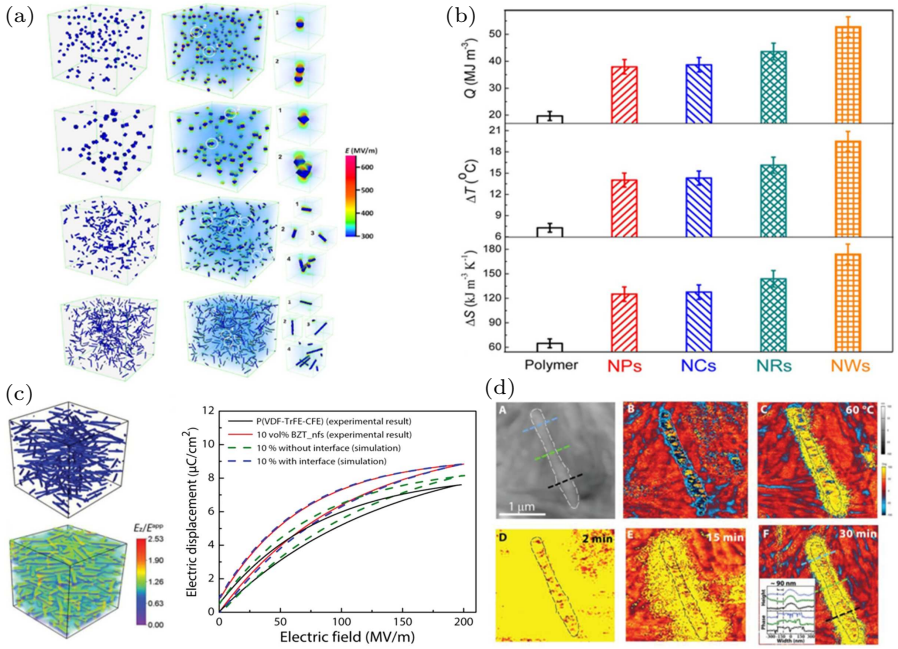


Fig. 6. (a) The electric field distribution in P(VDF-TrFE-CFE)/BST nanocomposites with different filler shapes was simulated using the phase-field method.[60] Copyright 2015, ACS. (b) Comparison of electrocaloric properties between nanocomposites filled with different shape nanofillers.[60] Copyright 2015, ACS. (c) Phase-field simulation of polarizability for nanocomposites.[63] Copyright 2018, Wiley. (d) *In-situ* PFM image of nanocomposites.[63] Copyright 2018, Wiley.

The synergistic effects of multi-phase fillers have also been demonstrated to achieve comprehensive enhancement of ECE performance. For example, through the synergistic effect of $Ba_{0.5}Ca_{0.5}Zr_{0.2}Ti_{0.8}O_3$ (BCZT) nanoparticles, boron nitride (BN) nanosheets, and $BiFeO_3$ (BFO) nanofibers, a ΔT of 13.5 K was achieved under an applied electric field of 220 MV/m, along

with an isothermal ΔS of 94.5 J·kg^{-1}·K^{-1}. Additionally, this composite was endowed with a breakdown field strength as high as 290 MV/m, which fully demonstrates the synergistic enhancement capability of multi-phase fillers in both electrocaloric and insulating properties (Figs. 7(a) and 7(b)).[72] In 2025, a study on PVDF/TiO_2 composites proposed the "strain-induced polar interface" mechanism, which clarifies the additional contribution of the all-trans conformation to interfacial polarization (Figs. 7(c) and 7(d)).[73]

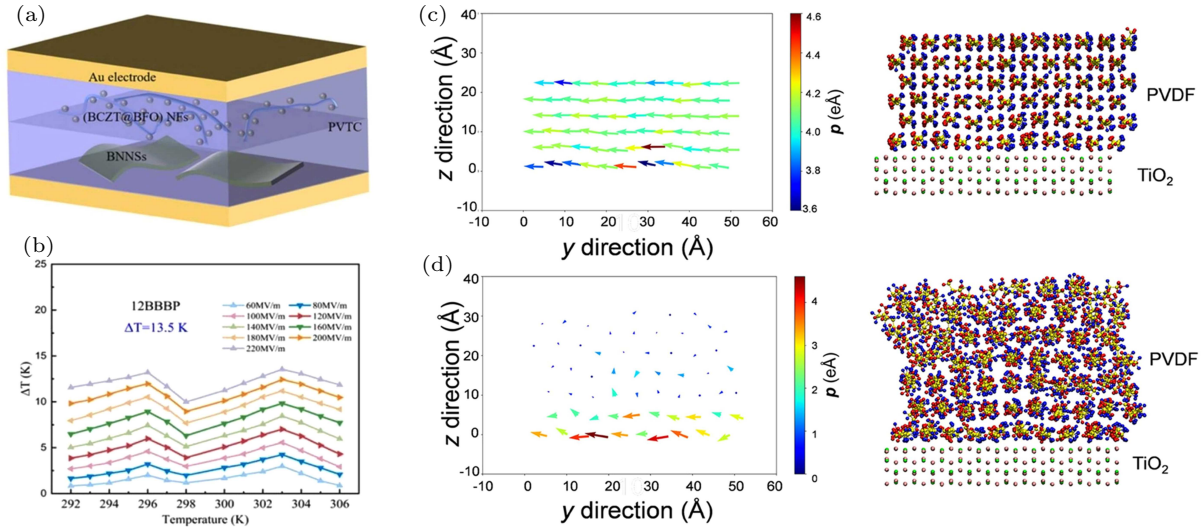


Fig. 7. (a), (b) Schematic diagram of synergistic effects of multi-form fillers.[72] Copyright 2024, Elsevier Inc. (c), (d) Molecular dynamics simulations on the interfacial polar phase induced by compressive strain.[73] Copyright 2025, Wiley.

For the synergistic enhancement of electrocaloric and thermal conductive properties, interfacial functionalization design plays a critical role. For instance, boron nitride nanosheets (BNNS) and BST were combined as a dual-functional filler and then composited with P(VDF-TrFE-CFE). As verified by thermocouple sensor measurements, this strategy maintained a ΔT of 35 K and simultaneously increased the composite's thermal conductivity by six times.[59] A three-dimensional silicon carbide (SiOC) ceramic network was first constructed via a sacrificial template method and then composited with P(VDF-TrFE-CFE); this composite exhibited excellent performance. Not only was the thermal conductivity of the composite increased by 12 times, but the polymer matrix was also induced into a mesoscopic-scale high-entropy state. Direct infrared thermography measurements were performed under a low applied electric field of 30 MV/m, and a ΔT of 2 K was detected, which fully demonstrates the synergistic effect between thermal conduction pathways and entropy regulation (Figs. 8(a) and 8(b)).[67] Notably, interfacial structure design can also induce mesoscopic-scale high-entropy states to enhance ECE. For example, a polar interface with ultra-high conformational entropy was constructed in P(VDF-TrFE-CFE) via a sacrificial template method, which enables the coexistence of multiple conformations and maximization of interfacial configurational entropy. This mesoscopic high-entropy interface contributes to a ΔS of 100 J·kg^{-1}·K^{-1} and a ΔT of 20 K under an applied electric field of 100 MV/m, establishing a new paradigm for interfacial entropy regulation in electrocaloric composites.[21] In another interfacial modification strategy, 3-sulfopropyl trimethoxysilane (SPTMS) molecules were covalently grafted onto BNNS and the ternary polymer (P(VDF-TrFE-CFE)), which enabled precise control over the interfacial spacing. Through this approach, the thermal conductivity of the composite was elevated to 0.72 W·m^{-1}·K^{-1}, and a significant ΔS was restored. This provides the first molecular-scale evidence for the feasibility of ordered–disordered synergy in electrocaloric composites (Figs. 8(c) and 8(d)).[74]

With the in-depth development of research, novel filler systems and macrostructural designs have further expanded the performance limits of polymer electrocaloric composites. For example, surface-functionalized graphene was combined with P(VDF-TrFE-CFE), and the composite was subjected to a stretching process. This process suppresses leakage current and enhances the polarization of the polymer matrix. When characterized using high-sensitivity thermal sensors, a ΔT of 5.2 K was achieved at an applied electric field of 40 MV/m.[62] Low-dielectric-constant nanodiamonds were composited with P(VDF-TrFE-CFE); the interfacial electric field distortion effect of these nanodiamonds promotes the polarization of the composite and reduces the phase transition energy barrier. As shown in Fig. 8(e), using an *in-situ* calibrated calorimeter, a ΔT of 10.7 K was achieved at 100 MV/m, which corresponds to a 60% improvement compared with the pure P(VDF-TrFE-CFE) matrix.[75] From a structural perspective, P(VDF-TrFE-CFE) nanowire arrays were embedded into a highly thermally

conductive anodic aluminum oxide (AAO) template. This structure enhances the flexibility and heat transfer capability of the material while maintaining strong electrocaloric–thermal coupling, which meets the application requirements of wearable devices (Fig. 8(f)).[23] The mesoscopically optimized multiphase structure (e.g., continuous polarization pathways, functionalized interfaces) provides a high-performance "material platform" for macroscopic regulation, as its enhanced polarization response and thermal conductivity reduce the dependence of macroscopic devices on extreme external fields.

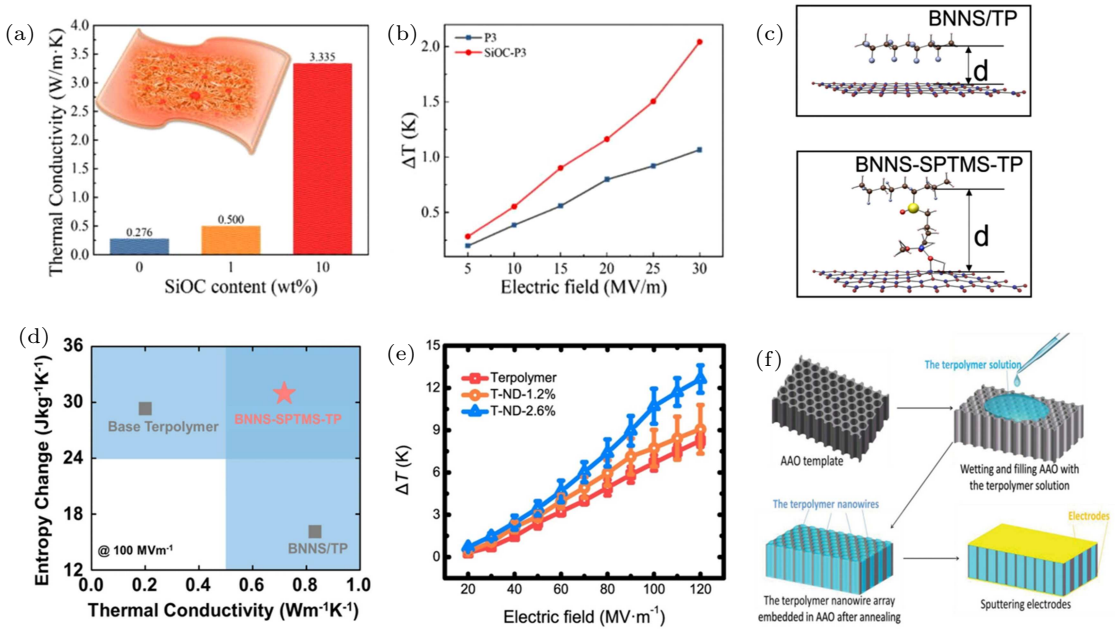


Fig. 8. (a), (b) Collaborative thermal management of the 3D thermal conductive ceramic EC composite films.[67] Copyright 2024, AIP Publishing. (c), (d) Schematic of BNNS-SPTMS-TP molecular structure design and ΔS under the electric field of 100 MV/m and thermal conductivity in the base terpolymer.[74] Copyright 2023, Elsevier Inc. (e) Schematic representation of the filling strategy for composites and ECE properties.[75] Copyright 2024, Springer Nature. (f) Schematic illustration of preparation of the polymer nanowire array.[23] Copyright 2018, Wiley.

3.3. Macro-scale engineering: structural optimization and external field synergy

Macro-scale regulation acts as the pivotal bridge for converting the microscale polarization advantages of electrocaloric materials into practical device cooling performance. Leveraging the mesoscopically optimized polarization and thermal conductivity, macroscopic strategies such as structural optimization and external field coupling further tune molecular chain orientation and interface polarization efficiency, ultimately unlocking the industrial application potential of electrocaloric composites while enhancing device reliability.

In terms of structural optimization, film thickness is a core parameter. According to the L–D theory, the adiabatic ΔT is positively correlated with ΔP^2. Thinning the polymer film shortens the charge migration distance and increases the breakdown field strength, allowing higher applied electric fields to be sustained and thus yielding a larger ΔP and ΔT. However, excessive thinning decreases the volume of active material, which in turn reduces the overall cooling capacity of the device. In practical applications, a balance between these factors must be achieved through a combination of experimental and simulation methods. For instance, P(VDF-TrFE) films are stacked into a multi-layer ceramic capacitor (MLCC) structure, which forms a series configuration that effectively reduces the required applied voltage. With this structure, a small applied voltage is sufficient to achieve a ΔT of 6.6 K. [76] Meanwhile, thermal treatments such as quenching and annealing exert a significant influence on material properties. Studies on P(VDF-TrFE-CFE) have shown that macro-scale quenching and low-temperature annealing reduce the crystalline size from 42 nm to 27 nm. This adjustment reduces the energy barrier for dipole orientation and improves low-field responsiveness, enabling the material to achieve a ΔT of 14.7 K at 150 MV/m and 30 °C while retaining the inherent flexibility of the polymer. This provides an efficient pathway for optimizing the performance of electrocaloric materials (Fig. 9(a)).[77]

External field coupling is another core macro-scale regulation strategy, which further optimizes molecular chain orientation and polarization anisotropy. As shown in Fig. 9(b), P(VDF-TrFE-CFE) films were subjected to uniaxial stretching under stress field control. This treatment modulates the material's microstructure by inducing the orientation of polymer chains into a polar all-trans conformation and enhancing crystalline order within the amorphous matrix. This stretching process induces the orientation of molecular chains along the stretching direction, enhances the order of crystals, and simultaneously increases polarization anisotropy and maximum ΔP, while also optimizing the internal phase interface (mesoscopic scale) induced by molecular chain orientation to reduce polarization loss. Notably, the effect of stretching on the ECE

is temperature-dependent: a 50% enhancement in ECE performance of the stretched samples (relative to unstretched counterparts) is achieved near the dielectric relaxation maximum temperature. At this temperature, the enhanced induced polarization compensates for the reduced orientational degeneracy of elementary dipolar entities arising from chain ordering. This finding provides a feasible strategy for the performance optimization of flexible electrocaloric devices, especially when operating near the material's dielectric relaxation maximum temperature.[53,78]

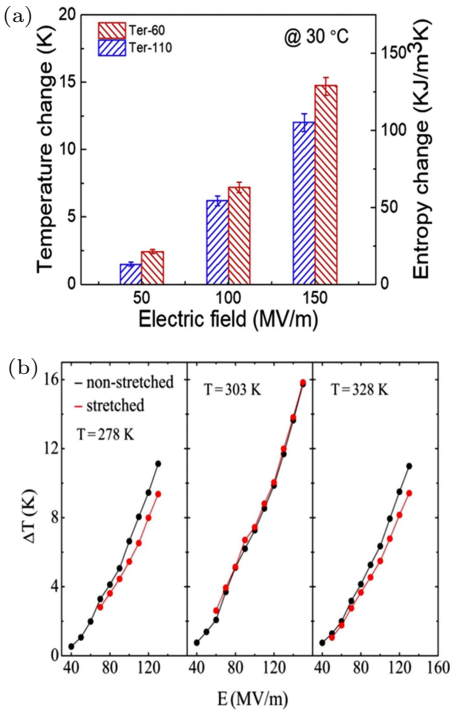


Fig. 9. (a) ΔT and ΔS at different annealing and quenching temperatures.[77] Copyright 2019, The Chinese Ceramic Society. (b) ECE properties for stretched and non-stretched terpolymer.[78] Copyright 2012, AIP Publishing.

4. EC cooling devices

The exploration and optimization of ECE performance in EC materials are targeted at developing refrigeration devices with superior cooling capabilities. An essential goal is to translate microscale ΔT enhancements into macroscopic cooling effects, and active electrocaloric regeneration (AER) serves as the mainstream technology to achieve this. AER is characterized by the reciprocal interaction between EC materials and a heat-transfer medium (either solid or fluid) to realize regenerative heat pumping, thereby extending the device temperature span beyond the intrinsic adiabatic ΔT of the material.[16,79]

Devices based on AER were initially developed using heat transfer fluids as the working medium. For instance, PVDF-based electrocaloric composites were coupled with silicone oil, and a ΔT of 3.3 K was achieved under an applied electric field of 50 MV/m. However, slight leakage of silicone oil was observed after 1000 cycles of operation, which led to a decrease in ΔT from 3.3 K to 2.1 K. Additionally, the volume occupied by fluid channels accounted for up to 40% of the total device volume, which impeded the miniaturization of the AER device.[80] To address these drawbacks, solid media have become the primary choice for polymer-based AER devices. In 2013, irradiated P(VDF-TrFE) electrocaloric films were stacked to form an MLCC structure (Fig. 10(a)), with stainless steel plates employed as the solid medium. The electrocaloric module was driven by a stepper motor to perform reciprocating motion (realizing the AER regeneration process), and the series configuration of the MLCC effectively reduced the required applied voltage, achieving a ΔT of 6.6 K even with a small applied voltage.[76]

Beyond AER-based systems, the flexibility of polymers facilitates the development of innovative non-AER electrocaloric devices, which are devoid of the AER-specific "regeneration" process and are highly compatible with applications such as wearable thermal management and on-chip thermal regulation. In 2017, a pioneering electrostatically actuated electrocaloric cooling device was designed (Fig. 10(b)). Electrostatic forces are employed to induce the vibration of polymer films for heat transfer, which enables the cooling film to reciprocate between the heat sink and heat source under an applied electric field of 60 MV/m and ultimately attain an adiabatic ΔT of 2.8 K. When attached to the back of a smartphone battery with an initial temperature of 52.5 °C, this non-AER device exhibited an 8 °C temperature drop within the first 5 seconds under an applied electric field of 66.7 MV/m and a frequency of 0.8 Hz. It significantly outperforms natural cooling, confirming its practical potential for wearable and on-chip applications (Fig. 10(c)).[79] In 2020, a self-actuated electrocaloric cooling fiber based on P(VDF-TrFE-CFE) was developed. Conductive fibers were used as core electrodes, and single-walled carbon nanotubes were employed as outer electrodes. The fiber realizes self-actuation through the piezoelectric effect that accompanies the electrocaloric effect, thus eliminating the requirement for external pumps or motors. Under an applied electric field of 100 MV/m, a ΔT of 0.7 K was achieved, providing a miniaturized solution for flexible wearable devices (Fig. 10(d)).[81] In 2022, a flexible microfluidic electrocaloric cooling capillary tube for chip cooling was developed, which for the first time enables the continuous generation of liquid media at temperatures below ambient within a sealed space.[82]

The cooling performance of single-stage AER devices remains constrained, while non-AER devices are also plagued by temperature span limitations. To address these drawbacks, cascaded structures have been extensively explored for non-AER devices. In 2020, the previously designed electrocaloric refrigeration device structure was further developed into a cascaded configuration. A four-layer cascaded device based

on P(VDF-TrFE-CFE) achieved a ΔT of 8.7 K under an applied electric field of 60 MV/m and a frequency of 1 Hz. Simulation results suggest that an eight-layer cascaded device could achieve a temperature span over 20 K (Fig. 10(e)).[11] In 2023, the ECE performance of flexible microfluidic capillaries was further optimized via a cascaded architecture (Fig. 10(f)). Specifically, a multi-stage cascaded structure was adopted to achieve cumulative cooling effects and sawtooth voltage regulation, thereby enhancing cooling power. At a liquid flow rate of 10 mm/s, a temperature span of 4.2 K was achieved, with a maximum temperature drop of 4.6 K. This system enables the sustainable delivery of sub-ambient liquid media, providing an efficient embedded thermal management solution for microelectronic systems.[83] A polymer film functionalized with dot-patterned electrodes was integrated into an electrostatically actuated cooling device, which enables precise point-to-point cooling. In chip-cooling experiments, this device effectively maintained the CPU surface temperature below 59.1 °C, delivering cooling performance on par with CPU air coolers while significantly outperforming desktop cooling fans (Fig. 10(g)).[84]

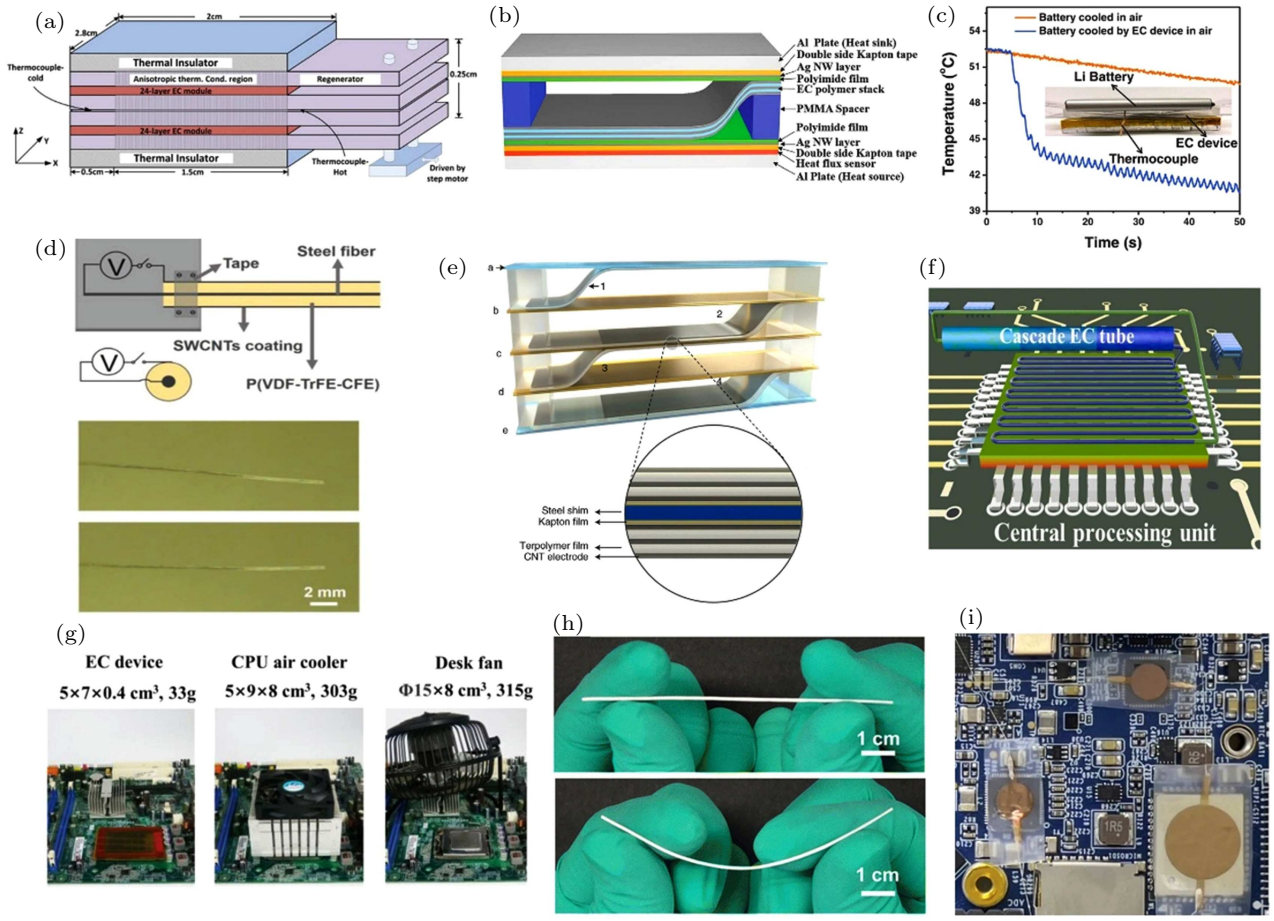


Fig. 10. The designed configuration of ECE devices based on polymer. (a) MLCC structure.[76] Copyright 2013, AIP Publishing. (b) and (c) A flexible EC cooling device powered by the electrostatic actuation mechanism.[79] Copyright 2017, The American Association for the Advancement of Science. (d) Schematic illustration of the self-actuation EC fiber.[81] Copyright 2020, Wiley. (e) Schematic illustration of a cascade EC cooling device containing four EC elements.[11] Copyright 2021, Elsevier Inc. (f) A flexible microfluidic capillary tube with a cascaded architecture for central processing unit cooling.[83] Copyright 2023, Elsevier Inc. (g) Size comparison of our pixel-matrix EC cooling device, CPU air cooler, and desk fan.[84] Copyright 2023, Wiley. (h) Optical photograph of flexible EC cooling capillary tube.[82] Copyright 2022, Elsevier Inc. (i) Photograph of the on-chip EC cooling refrigerator.[85] Copyright 2024, Springer Nature.

Recent advancements in non-AER device architectures have broadened the application scope of EC technology, expanding it from passive cooling to multifunctional and miniaturized solutions. In 2024, a chip-scale flexible non-AER cooling device was developed (Fig. 10(h)), which achieves an instantaneous additional temperature reduction of 17.5 K compared to passive thermal management solutions, benefiting from molecular-scale high-entropy design for low-field polarization enhancement and mesoscopic SiOC ceramic networks for efficient heat conduction (Fig. 10(i)).[85] A separate study leveraged the synergistic effect between the electrocaloric effect and Joule heating to realize ultrafast thermal camouflage based on pixel arrays. This technology covers the visible-to-infrared multiband spectrum, with a temperature change rate of 3.8×10^{-3} K/s, and opens up new application avenues for electrocaloric materials in dynamic thermal management and

adaptive camouflage.[86] A dual-functional device based on EC composite materials was also designed. Electrostatic actuation drives the device stack to reciprocate between a simulated CPU and a heat sink, which not only cools an overheated CPU from 80 °C to 42 °C within 120 seconds but also recovers waste heat with an energy density of 1.33 J/cm^3. After 10^4 cycles, the device retained stable performance and exhibited a significantly smaller footprint than conventional desktop fans and CPU air coolers, thereby delivering a dual-functional solution for compact thermal management in electronic devices.[87]

In summary, the advancement of EC cooling devices proceeds along two complementary pathways: the optimization of AER devices to maximize temperature span, and the exploration of diverse innovative non-AER architectures for applications requiring miniaturization, flexibility, or multifunctional integration.

5. Conclusion and perspectives

Electrocaloric refrigeration technology is recognized as a highly promising solid-state cooling solution. Over the past decade, various high-performance EC materials ($\Delta T > 10$ K) have been developed. Among these materials, electrocaloric polymer nanocomposites hold great promise for simultaneously realizing a substantial ECE, high thermal conductivity, and excellent mechanical flexibility, properties that are difficult to achieve with inorganic or organic materials alone.

To systematically meet these performance requirements, this review synthesizes and establishes a coherent multi-scale design framework for polymer nanocomposites based on recent advances in the field. The core framework consists of three interlinked layers: (1) molecular-scale engineering (e.g., defect regulation, high-entropy design) to tailor dipole responsiveness; (2) mesoscale interface engineering to synergistically enhance polarization and thermal conductivity; and (3) macroscale device optimization for efficient heat exchange. Based on this framework, significant advancements have been attained: multi-scale synergistic regulation, including molecular defect tuning, high-entropy design, mesoscale interface modification, and macroscale external field coupling, has substantially improved material performance. Concurrently, diverse electrocaloric refrigeration devices have been successfully demonstrated, validating their applicability in wearable thermal management and chip hotspot cooling.

Nevertheless, critical challenges persist for efficient commercialization, particularly in material properties. While structures like MLCC help reduce operating voltage, the intrinsic low-field ECE performance of these materials still requires further improvement. The molecular-scale strategies discussed in Section 3 (e.g., high-entropy design) are fundamentally targeted at boosting dipole responsiveness under low electric fields, which has been demonstrated to enhance the low-field ΔT of P(VDF-TrFE-CFE)-based nanocomposites by over 30% in recent studies, but the relationship between polymer chain structure and ECE performance remains unclear. Additionally, the fundamental mechanism underlying interface engineering remains debated. Separately, the mesoscale interface engineering detailed in Section 3 addresses another key bottleneck, polymers' intrinsic low thermal conductivity, by constructing efficient thermal conduction networks.

Beyond thermal conductivity enhancement, stability and scalability are also pivotal for industrialization. The fatigue and aging mechanisms of materials under long-term, high-electric-field cycling need to be investigated in depth. The path from laboratory-scale samples to large-scale production remains lengthy, with challenges (e.g., uniform dispersion of nanofillers) yet to be addressed.

In terms of device performance, the current maximum cooling temperature span is approximately 17.5 K, which still falls short of the 25 K temperature span required for commercial refrigeration. The development of compact, efficient, and reliable device architectures is of crucial importance.

Future Perspectives: Building on the summarized design strategies, future research endeavors should shift from general principles to targeted investigations:

1. Low-field performance. Adopt machine learning-guided polymer chain design (e.g., high-entropy design) to flatten energy landscapes.

2. Thermal conductivity. Engineer hierarchical filler architectures with covalently bonded interfaces to minimize interfacial thermal resistance.

3. Device efficiency. Develop asymmetric regenerator configurations to optimize the utilization of intrinsic material properties.

4. Stability. Establish structure–property–fatigue correlations with a focus on interface evolution mechanisms.

In conclusion, high operating electric fields, inadequate material performance under low fields, and narrow operating temperature ranges remain key bottlenecks. Future research should focus on deepening the quantitative understanding and practical implementation of the multi-scale strategies outlined herein, thereby promoting the commercialization of electrocaloric refrigeration technology.

Acknowledgements

This work was supported by the National Natural Science Foundation of China (Grant Nos. 523B2011, 52372108, and 52272110), the Fundamental Research Funds for the Central Universities (Grant No. 5003190024), the Natural Science Foundation of Hubei Province (Grant No. 2024AFA012), and the National Key Research and Development Program of China (Grant No. 2022YFA1204603). We would also like to thank the Analytical and Testing Center of HUST.

References

[1] Wetzel D and Cozzi L 2022 *International Energy Agency*, December, 2021 Paris, France, p. 11
[2] Shah N and Phadke A 2015 *Lawrence Berkeley National Laboratory,* November, 2015 Paris, France, p. 1
[3] Veldersa G J M, Faheyb D W, Danielb J S, McFarlandc M and Andersen S O 2009 *Proc. Natl. Acad. Sci. USA* **106** 10949
[4] Russ B, Glaudell A, Urban J J, Chabinyc M L and Segalman R A 2016 *Nat. Rev. Mater.* **1** 16050
[5] Franco V, Blázquez J S, Ipus J J, Law J Y, Moreno-Ramírez L M and Conde A 2018 *Prog. Mater Sci.* **93** 112
[6] Mischenko A S, Zhang Q M, Scott J F , Whatmore R W and Mathur N D 2006 *Science* **311** 1270
[7] Neese B, Chu B, Lu S G, Wang Y, Furman E and Zhang Q M 2008 *Science* **321** 821
[8] Tušek J, Engelbrecht K, Eriksen D, Dall'Olio S, Tušek J and Pryds N 2016 *Nat. Energy* **1** 16134
[9] Tu Y D, Wang R Z, Zhang Y N and Wang J Y 2018 *Joule* **2** 1452
[10] Zhai Y, Ma Y G, David S N, Zhao D L, Lou R N, Tan G, Yang R G and Yin X B 2017 *Science* **355** 1062
[11] Meng Y, Pu J H and Pei Q B 2021 *Joule* **5** 780
[12] Sun Q D, Zhi G, Zhou S, Dong X, Shen Q Y, Tao R and Qi J F 2024 *Adv. Mater. Technol* **9** 2400263
[13] Nair B, Usui T, Crossley S, Kurdi S, Guzmán-Verri G G, Moya X, Hirose S and Mathur N D 2019 *Nature* **575** 468
[14] Von P K and I.Kurtschatov 1930 *Eingegangen* **2** 192
[15] Wang Z M, Hou H C, Xue H W, Ji Z Q, Zhang H and Wang X Y 2025 *J. Mater. Chem. C* **13** 18009
[16] Shi J Y, Han D L, Li Z C, Yang L, Lu S G, Zhong Z F, Chen J P, Zhang Q M and Qian X S 2019 *Joule* **3** 1200
[17] Kumar A, Thakre A, Jeong D Y and Ryu J 2019 *J. Mater. Chem. C* **7** 6836
[18] Cai Y, Li Q, Du F H, Feng J W, Han D L, Zheng S Y, Yang S H, Zhang Y J, Yu B B, Shi J Y and Qian X S 2022 *Front. Energy* **17** 450
[19] Qian X S, Chen X, Zhu L and Zhang Q M 2023 *Science* **380** 1
[20] Cui H, He W, Pei Q B and Ma R J 2022 *Organic Ferroelectric Materials and Applications* (Woodhead Publishing Series in Electronic and Optical Materials) p. 535
[21] Zheng S Y, Du F H, Zheng L R, Han D L, Li Q, Shi J Y, Chen J P, Shi X M, Huang H B, Luo Y R, Yang Y R, O'Reilly P, Wei L L, Souza N D, Hong L and Qian X S 2023 *Science* **382** 1020
[22] Qian X S, Han D L, Zheng L R, Chen J, Tyagi M, Li Q, Du F H, Zheng S Y, Huang X Y, Zhang S H, Shi J Y, Huang H B, Shi X M, Chen J P, Qin H C, Bernholc J, Chen X, Chen L Q, Hong L and Zhang Q M 2021 *Nature* **600** 664
[23] Zhang G Z, Weng L X, Hu Z Y, Liu Y, Bao R X, Zhao P, Feng H, Yang N, Li M Y, Zhang S L, Jiang S L and Wang Q 2019 *Adv. Mater.* **31** 1806642
[24] Zhang G Z, Zhang X S, Huang H B, Wang J J, Li Q, Chen L Q and Wang Q 2016 *Adv. Mater.* **28** 4811
[25] Zhang. Q M and Zhang T 2017 *Science* **357** 1094
[26] Chen X, Zhu W Y and Zhang Q M 2023 *iEnergy.* **2** 100
[27] Lines M E and Glass A M 2001 *IEEE J. Quantum Electron.* **14** 450
[28] Lines M E, Glass A M and Burns G 1978 *Phys. Today* **31** 56
[29] Rožič B, Kosec M, Uršič H, Holc J, Malič B, Zhang Q M, Blinc R, Pirc R and Kutnjak Z 2011 *J. Appl. Phys.* **110** 064118
[30] Li X Y, Lu S G, Chen X Z, Gu H M, Qian X S and Zhang Q M 2013 *J. Mater. Chem. C* **1** 23
[31] Lu S G and Zhang Q M 2009 *Adv. Mater.* **21** 1983
[32] Jia Y B and Sungtaek Ju Y 2013 *Appl. Phys. Lett.* **103** 042903
[33] Sanlialp M, Shvartsman V V, Faye R, Karabasov M O, Molin C, Gebhardt S, Defay E and Lupascu D C 2018 *Rev. Sci. Instrum.* **89** 034903
[34] Sanlialp M, Shvartsman V V, Acosta M, Dkhil B and Lupascu D C 2015 *Appl. Phys. Lett.* **106** 062901
[35] Baba M, Kuwahara R, Ishibashi N, Fukuda S and Takeda M 2021 *Rev. Sci. Instrum.* **92** 044902
[36] Usui T, Hirose S, Ando A, Crossley S, Nair B, Moya X and Mathur N D 2017 *J. Phys. D: Appl. Phys.* **50** 424002
[37] Jia Y B and Ju Y S 2014 *Appl. Phys. Lett.* **104** 251913
[38] Qian J F, Hu P H, Liu C, Jiang J Y, Dan Z K, Ma J, Lin Y H, Nan C W and Shen Y 2018 *Sci. Bull* **63** 356
[39] Pandya S, Wilbur J D, Bhatia B, Damodaran A R, Monachon C, Dasgupta A, King W P, Dames C and Martin L W 2017 *Phys. Rev. Appl* **7** 034025
[40] Spièce J, Fonck V, Evangeli C, Dobson P S, Weaver J M R and Gehring P 2025 *Small Methods* **9** 2401715
[41] Lu S G, Rožič B, Zhang Q M, Kutnjak Z and Neese B 2011 *Appl. Phys. Lett.* **98** 122906
[42] Liu Y, Zhang B, Xu W H, Haibibu A, Han Z B, Lu W C, Bernholc J and Wang Q 2020 *Nat. Mater.* **19** 1169
[43] Yao Y T, Hou G H, Li N N, Zhou T Y, Liu L W, Liu Y J and Leng J S 2016 *J. Appl. Polym. Sci.* **134** 44413
[44] Liu Y, Haibibu A, Xu W H, Han Z B and Wang Q 2020 *Adv. Funct. Mater.* **30** 2000648
[45] Moreira R L 2013 *Ferroelectrics* **446** 820971
[46] Li X Y, Qian X S, Gu H M, Chen X Z, Lu S G, Lin M R, Bateman F and Zhang Q M 2012 *Appl. Phys. Lett.* **101** 132903
[47] Liu Y, Zhou Y, Qin H C, Yang T N, Chen X, Li L, Han Z B, Wang K, Zhang B, Lu W C, Chen L Q, Bernholc J and Wang Q 2023 *Nat. Mater.* **22** 873
[48] Lu S G, Rožič B, Zhang Q M, Kutnjak Z, Li X, Furman E, Gorny L J, Lin M, Malič B, Kosec M, Blinc R and Pirc R 2010 *Appl. Phys. Lett.* **97** 162904
[49] Chen X, Xu W H, Lu B, Zhang T, Wang Q and Zhang Q M 2018 *Appl. Phys. Lett.* **113** 113902
[50] Rui G C, Zhu W Y, Li L, Lee J, Guo Y W, Zou Q, Wu S Y, Li R P, Lannuzel T, Domingues Dos Santos F, Aubart M A, Kim S H, Chen L Q, Zhu L, Liu Z K and Zhang Q M 2025 *Small Sci.* **5** 2400624
[51] Luo Q, Guo Z J and Shen B L 2025 *Matter* **8** 102287
[52] Han D L, Zhao Y F and Qian X S 2025 *Thermo-X* **1** 202505
[53] Li X Y, Qian X S, Lu S G, Cheng J P, Fang Z and Zhang Q M 2011 *Appl. Phys. Lett.* **99** 052907
[54] Lu B, Chen X, Zhang T, Lu S G and Zhang Q M 2018 *Appl. Phys. Lett.* **113** 153903
[55] Qian X S, Ye H J, Yang T N, Shao W Z, Zhen L, Furman E, Chen L Q and Zhang Q M 2015 *Adv. Funct. Mater.* **25** 5134
[56] Chen X Z, Li X, Qian X S, Wu S, Lu S G, Gu H M, Lin M, Shen Q D and Zhang Q M 2013 *Polymer* **54** 2373
[57] Li Q, Zhang G Z, Zhang X S, Jiang S L, Zeng Y K and Wang Q 2015 *Adv. Mater.* **27** 2236
[58] Zhang G Z, Li Q, Gu H M, Jiang S L, Han K, Gadinski M R, Haque M A, Zhang Q M and Wang Q 2015 *Adv. Mater.* **27** 1450
[59] Zhang G Z, Fan B Y, Zhao P, Hu Z Y, Liu Y, Liu F H, Jiang S L, Zhang S L, Li H L and Wang Q 2018 *ACS Appl. Energy Mater.* **1** 1344
[60] Zhang G Z, Zhang X S, Yang T N, Li Q, Chen L Q, Jiang S L and Wang Q 2015 *ACS Nano* **9** 7164
[61] Jiang Z Y, Zheng X C and Zheng G P 2015 *RSC Adv.* **5** 61946
[62] Yang L, Qian X S, Koo C, Hou Y, Zhang T, Zhou Y, Lin M R, Qiu J H and Zhang Q M 2016 *Nano Energy* **22** 461
[63] Qian J F, Peng R C, Shen Z H, Jiang J Y, Xue F, Yang T N, Chen L Q and Shen Y 2018 *Adv. Mater.* **31** 1801949
[64] Chen Y Q, Qian J F, Yu J Y, Guo M F, Zhang Q H, Jiang J Y, Shen Z H, Chen L Q and Shen Y 2020 *Adv. Mater.* **32** 1907927
[65] Lu Y C, Yu J Y, Huang J Y, Yu S H, Zeng X R, Sun R and Wong C P 2019 *Appl. Phys. Lett.* **114** 233901
[66] Zou K L, Shao C C, Bai P J, Zhang C, Yang Y, Guo R D, Huang H B, Luo W, Ma R J, Cao Y, Sun A X, Zhang G Z and Jiang S L 2022 *Nano Lett.* **22** 6560
[67] Wang F, Wu W L, Wu M, Zhou D S, Wang X L and Shen Q D 2024 *Appl. Phys. Lett.* **124** 152903
[68] Rožič B, Kutnjak Z, Neese B, Guo. L S and Zhang Q M 2010 *Phase Transitions* **83** 819
[69] Qian X S, Yang T N, Zhang T, Chen L Q and Zhang Q M 2016 *Appl. Phys. Lett.* **108** 142902
[70] Xu H and Huang J 2025 *Chin. Phys. B* **34** 067702
[71] Morozovska A N, Eliseev E A, Glinchuk M D, Shevliakova H V, Svechnikov G S, Silibin M V, Sysa A V, Yaremkevich A D, Morozovsky N V and Shvartsman V V 2019 *Phys. Rev. Mater* **3** 104414
[72] Zhao M, Sun X F, Ji P Q, Li T F, Lu Y Z, Ma L G, Xu C P, Jiao S L, Dai J Q, Wu Y Z, Cai H L and Wu X S 2024 *Nano Energy* **128** 1
[73] Li C Y, Qin H C, Zhou Y, Yang T N, Chen X, Li L, Yuan Z, Wang K, Zhang B, Lu W C, Chen L Q, Liu Y, Bernholc J and Wang Q 2025 *Adv. Funct. Mater.* **35** 2421825
[74] Han D L, Du F H, Zhang Y J, Zheng L R, Chen J, Huang X Y, Li Q, Zheng S Y, Shi J Y, Chen J P, Dong J J and Qian X S 2023 *Joule* **7** 2174

[75] Li Q, Wei L Q, Zhong N, Shi X M, Han D L, Zheng S Y, Du F H, Shi J Y, Chen J P, Huang H B, Duan C G and Qian X S 2024 *Nat. Commun.* **15** 702
[76] Gu H M, Qian X S, Li X Y, Craven B, Zhu W Y, Cheng A, Yao S C and Zhang Q M 2013 *Appl. Phys. Lett.* **102** 122904
[77] Qian J F, Jiang J Y and Shen Y 2019 *J. Materiomics* **5** 357
[78] Bobnar V, Li X, Casar G, Eršte A, Glinšek S, Qian X and Zhang Q M 2012 *J. Appl. Phys.* **111** 083515
[79] Ma R J, Zhang Z Y, Tong K, Huber D, Kornbluh R, Ju Y S and Pei Q B 2017 *Science* **357** 1130
[80] Plaznik U, Kitanovski A, Rožič B, Malič B, Uršič H, Drnovšek S, Cilenšek J, Vrabelj M, Poredoš A and Kutnjak Z 2015 *Appl. Phys. Lett.* **106** 043903
[81] Wang H L, Meng Y, Zhang Z Y, Gao M, Peng Z H, He H C and Pei Q B 2020 *Adv. Energy Mater.* **10** 1903902
[82] Cui H, Zhang Q, Bo Y W, Bai P J, Wang M Y, Zhang C Y, Qian X S and Ma R J 2022 *Joule* **6** 258
[83] Bai P J, Cui H, Zhang D, Bo Y W, Liu L L and Ma R J 2023 *Next Materials* **1** 873
[84] Bai P J, Zhang Q, Cui H, Bo Y W, Zhang D, He W, Chen Y S and Ma R J 2023 *Adv. Mater.* **35** 2209181
[85] Han D L, Zhang Y J, Huang C L, Zheng S Y, Wu D Y, Li Q, Du F H, Duan H X, Chen W L, Shi J Y, Chen J P, Liu G, Chen X and Qian X S 2024 *Nature* **629** 1041
[86] Bo Y W, Zhang Q, Bai P J, Cui H, Liu L L, Wang G F, Wang L T, Yuan S H, Zhou Z X and Ma R J 2024 *Joule* **8** 2160
[87] Zou K L, Bai P J, Li K H, Luo F Y, Liang J J, Lin L, Ma R J, Li Q, Jiang S L, Wang Q and Zhang G Z 2024 *Nat. Commun.* **15** 6670